IxV Curves of Boron and Nitrogen Doping Zigzag Graphene Nanoribbons

JOSÉ E. PADILHA,[1] RENATO B. PONTES,[1] ANTÔNIO J. R. DA SILVA,[1,2] ADALBERTO FAZZIO[1,3]

[1]*Instituto de Física, Universidade de São Paulo, CP 66318, 05315-970, São Paulo, SP, Brazil*
[2]*Laboratório Nacional de Luz Síncrotron, CP 6192, 13083-970, Campinas, SP, Brazil*
[3]*Centro de Ciências Naturais e Humanas, Universidade Federal do ABC, Santo André, SP, Brazil*

Received 23 December 2009; accepted 22 February 2010
Published online 29 June 2010 in Wiley Online Library (wileyonlinelibrary.com).
DOI 10.1002/qua.22690

ABSTRACT: We investigate the transport properties (IxV curves and zero bias transmittance) of pristine graphene nanoribbons (GNRs) as well as doped with boron and nitrogen using an approach that combines nonequilibrium Green's functions and density functional theory (DFT) [NEGF-DFT]. Even for a pristine nanoribbon we verify a spin-filter effect under finite bias voltage when the leads have an antiparallel magnetization. The presence of the impurities at the edges of monohydrogenated zigzag GNRs changes dramatically the charge transport properties inducing a spin-polarized conductance. The IxV curves for these systems show that depending on the bias voltage the spin polarization can be inverted. © 2010 Wiley Periodicals, Inc. Int J Quantum Chem 111: 1379–1386, 2011

Key words: graphene; charge transport; nanoribbons

Introduction

Graphene nanoribbons (GNRs), which are thin strips of graphene [1–3], have been widely studied not only because of their interesting physical characteristics but because they also present great technological potential [4, 5]. The physical properties of these 2D structures such as low noise, large values for magnetoresistance and high electrical and thermal conductivity make the GNRs a possible alternative for devices in general [6–9].

The electronic properties of the nanoribbons widely depend on the edge structures (armchair or zigzag). GNRs with controlled edge orientation have been fabricated by Scanning Tunneling Microscope (STM) lithography [10]. Among the properties of these ribbons that depend on the edge structure, is the prediction that zigzag nanoribbons will present magnetic order due to the spin polarization at the edges.

Correspondence to: A. J. R. Da Silva; e-mail: ajrsilva@if.usp.br
Contract grant sponsor: CAPES.
Contract grant sponsor: CNPq.
Contract grant sponsor: FAPESP (Brazilian agencies).

One way to modify the structural, electronic and transport properties of a material is through doping [11, 12]. In semiconductors, for example, the addition of a small number of impurities, i.e., dopant atoms, can greatly change its conductivity. In type-IV semiconductors, for example, boron is a p-type dopant since it introduces acceptor levels, or "holes" in the system. Nitrogen doping type-IV semiconductors has also been studied because it is an n-type dopant introducing a donor level in the system. The role of a single nitrogen atom and complex doping type-IV semiconductors was studied in [13].

Understanding the effect of doping in nanostructures, such as graphene nanorribons, is thus an important issue. In a recent work [14], it was verified that boron doping a GNR causes a local distortion in the lattice and generates distinct charge transport for each spin channel, which would allow the use of these nanorribbons as a spin filter. In this work, we present IxV curves for a (3,0) zigzag GNR doped with boron and nitrogen, extending the previous zero-bias transport calculations. We also present IxV calculations for pristine ferromagnetic (FM) and antiferromagnetic (AFM) graphene zigzag nanorribons. The Ezawa's notation was used to classify the nanoribbon [15].

Methodology

We performed spin-polarized total energy *ab initio* calculations within the density functional theory (DFT) framework [16, 17] to determine the structural, electronic and transport properties of a pristine (3,0) zigzag GNR. The calculations were done using the generalized gradient approximation (GGA) for the exchange-correlation term as proposed by Perdew et al. [18] Troullier-Martins norm-conserved pseudopotentials [19] were used to describe the interaction between the valence and core electrons. The calculations were performed with the SIESTA code [20]. A double-ς basis set plus a polarization function (DZP) was employed and an energy cutoff of 200 Ry for the grid integration was used to represent the charge density. The structures were considered relaxed when the residual forces in all atoms were smaller than 0.03 eV/Å. A sample of $1 \times 1 \times 10$ k-points (z-direction along the GNR growth direction) chosen by the method of Monkhorst-Pack was used to describe the Brillouin zone [21].

The transport properties were obtained using the nonequilibrium Green's function, where the Hamiltonian matrix is generated through DFT (NEGF-DFT) [22]. For the electron transport through the magnetic contact we modified the TRANSAMPA [23] code. The system was divided in three parts: left electrode (LL), central region (CC) and right electrode (RR). The central region (CC), contains the left and right buffers that are regions with bulk-like character as well as the scattering region itself, which contains the system under investigation (see Fig. 1). We also assume that the electrodes only couple with the central region (CC), but not with each other. In other words, the left electrode does not couple with the right electrode.

Once the Hamiltonian and overlap matrices are calculated, we can write down the equations for the Green's functions as

$$\begin{pmatrix} ES_{LL}-H_{LL} & ES_{LC}-H_{LC} & 0 \\ ES_{CL}-H_{CL} & ES_{CC}-H_{CC} & ES_{CR}-H_{CR} \\ 0 & ES_{RC}-H_{RC} & ES_{RR}-H_{RR} \end{pmatrix} \times \begin{pmatrix} g_{LL} & g_{LC} & g_{LR} \\ g_{CL} & g_{CC} & g_{CR} \\ g_{RL} & g_{RC} & g_{RR} \end{pmatrix} = \begin{pmatrix} \mathbf{1} & 0 & 0 \\ 0 & \mathbf{1} & 0 \\ 0 & 0 & \mathbf{1} \end{pmatrix} \quad (1)$$

which can be solved to obtain the Green's function of the scattering region g_{CC}

$$g_{CC}(E) = (ES_{CC} - H_{CC} - \Sigma_L(E) - \Sigma_R(E))^{-1} \quad (2)$$

where we have introduced the "self-energies" of the electrodes $\Sigma_L(E)$ and $\Sigma_R(E)$, which describe the influence of the electrodes on the electronic structure of the device. These quantities can be calculated from the surface Green's functions of the isolated left and right semi-infinite electrodes (these are the elements of the whole electrodes Green's functions that interact with the central region due to the localized nature of the coupling matrices):

$$g_{LL}(E) = (ES_{LL} - H_{LL})^{-1} \quad (3)$$

$$g_{RR}(E) = (ES_{RR} - H_{RR})^{-1} \quad (4)$$

as

$$\Sigma_L(E) = (ES_{LC} - H_{LC})g_{LL}(E)(ES_{CL} - H_{CL}) \quad (5)$$

$$\Sigma_R(E) = (ES_{RC} - H_{RC})g_{RR}(E)(ES_{CR} - H_{CR}) \quad (6)$$

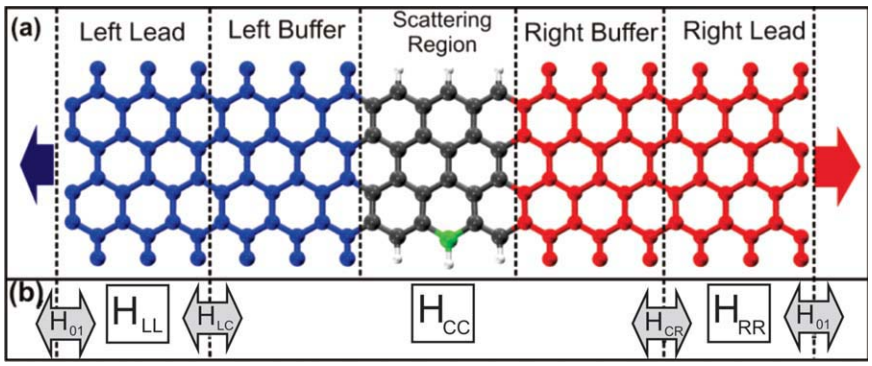

FIGURE 1. (a) Schematic representation of the system used in the transport calculations. The device is composed by left/right (L/R) bulk electrodes and a scattering region (CC), which is connected to the leads by a buffer region (Left Buffer and Right Buffer). The green atom marks the energetically most stable position for N and B substitutional doping. (b) Structure of the system in terms of the Hamiltonian matrices. [Color figure can be viewed in the online issue, which is available at wileyonlinelibrary.com.]

The surface Green's functions of the electrodes are obtained via a recursive algorithm as described in [23]. Finally, we can define the coupling matrices that allow us to calculate the transmission function:

$$\Gamma_{\mathrm{L}}(\mathrm{E}) = \mathrm{i}(\Sigma_{\mathrm{L}}(\mathrm{E}) - \Sigma_{\mathrm{L}}^{\dagger}(\mathrm{E})) \tag{7}$$

$$\Gamma_{\mathrm{R}}(\mathrm{E}) = \mathrm{i}(\Sigma_{\mathrm{R}}(\mathrm{E}) - \Sigma_{\mathrm{R}}^{\dagger}(\mathrm{E})). \tag{8}$$

Using the relations described above we can write the transmittance of the system for a ballistic process as:

$$T(E) = Tr[\Gamma_{\mathrm{L}} g_{\mathrm{CC}}^{\mathrm{A}} \Gamma_{\mathrm{R}} g_{\mathrm{CC}}^{\mathrm{R}}]. \tag{9}$$

If there is no external bias applied to the system, it is on the linear response regime, and the transport properties of the system can be directly obtained as described earlier.

When an external bias is applied, the charge density on the scattering region will be different than on the equilibrium situation. On the electrodes we assume that the external bias will only cause a rigid shift of the eigenvalues. The Hamiltonian of the whole system with an applied bias can be written as:

$$\boldsymbol{H} = \begin{pmatrix} \boldsymbol{H}_{\mathrm{LL}} + \boldsymbol{S}_{\mathrm{L}} eV/2 & \boldsymbol{H}_{\mathrm{LC}} & \mathbf{0} \\ \boldsymbol{H}_{\mathrm{CL}} & \boldsymbol{H}_{\mathrm{CC}} & \boldsymbol{H}_{\mathrm{CR}} \\ \mathbf{0} & \boldsymbol{H}_{\mathrm{RC}} & \boldsymbol{H}_{\mathrm{RR}} - \boldsymbol{S}_{\mathrm{R}} eV/2 \end{pmatrix} \tag{10}$$

As the Hamiltonian of the system depends on the density matrix, it needs to be calculated self-consistently using the Green's function in the presence of the external bias. This density matrix can be calculated using the lesser Green's function [24–26]:

$$\rho = \frac{l}{2\pi i} \int dE \boldsymbol{g}^{<}(E) \tag{11}$$

where $\boldsymbol{g}^{<}$ is given by:

$$\boldsymbol{g}^{<}(E) = \boldsymbol{g}^{R}(E) \Sigma^{<}(E) \boldsymbol{g}^{A}(E) \tag{12}$$

and $\Sigma^{<}$ is calculated by:

$$\Sigma^{<}(E) = i[\Gamma_{\mathrm{L}} f(E - \mu_{\mathrm{L}}) + \Gamma_{\mathbf{R}} f(E - \mu_{\mathrm{R}})]. \tag{13}$$

The lesser green's function can be written as:

$$\boldsymbol{g}^{<}(E) = i\boldsymbol{g}^{R}(E)[\Gamma_{\mathrm{L}} f(E - \mu_{\mathrm{L}}) + \Gamma_{\mathbf{R}} f(E - \mu_{\mathrm{R}})]\boldsymbol{g}^{A}(E) \tag{14}$$

The self-consistent procedure follows as:

1. First we calculate a trial charge density—$\rho^{0}(\boldsymbol{r}) = \langle \boldsymbol{r} \,|\, \rho_{\mathrm{C}}^{0} \,|\, \boldsymbol{r} \rangle$—which is used to calculate the Hamiltonian matrix elements;
2. $\boldsymbol{g}_{\mathrm{CC}}^{R}$, Γ_{L}, and Γ_{R} are calculated using the Eqs. (2), (7), and (8), respectively;
3. Once $\boldsymbol{g}_{\mathrm{CC}}^{R}$, Γ_{L}, and Γ_{R} are calculated, we use them to calculate $\boldsymbol{g}^{<}(E)$ via Eq. (14), which is replaced in Eq. (11) to obtain the new density matrix;
4. This procedure is repeated until a self-consistent solution is obtained, which is reached when $Max \,|\, \rho^{i} - \rho^{i+1} \,| < \delta$, where $\delta \ll 1$ is the convergence criterion.

Following the Landauer formula in the Meier-Wingreen procedure [27] the current can be written as:

$$I = \frac{2e^2}{h}\int dE Tr\Big[\Gamma_L(E,V)g^A_{CC}(E,V)\Gamma_R(E,V)g^R_{CC}(E,V)\Big]\Big(f(E-\mu_L)-f(E-\mu_R)\Big), \quad (15)$$

where $\mu_{L/R} = \mu \pm$ eV, and $f(E - \mu_{L/R})$ is the Fermi function for a given temperature (T). The transmittance under an external bias is given by:

$$T(E,V) = Tr[\Gamma_L(E,V)g^A_{CC}(E,V)\Gamma_R(E,V)g^R_{CC}(E,V)]. \quad (16)$$

SPIN-DEPENDENT TRANSPORT

We have generalized the formalism described earlier to include magnetic systems (i.e., nonspin-degenerate states). The Hamiltonian and the Green's function of the device are now spin-dependent, and the spin-dependent matrices can be written as:

$$H_{CC} = \begin{pmatrix} H^{\uparrow\uparrow}_{CC} & H^{\uparrow\downarrow}_{CC} \\ H^{\downarrow\uparrow}_{CC} & H^{\downarrow\downarrow}_{CC} \end{pmatrix}. \quad (17)$$

$$g_{CC}(E) = \begin{pmatrix} g^{\uparrow\uparrow}_{CC} & g^{\uparrow\downarrow}_{CC} \\ g^{\downarrow\uparrow}_{CC} & g^{\downarrow\downarrow}_{CC} \end{pmatrix}. \quad (18)$$

If we assume that there are no mechanisms for spin-mixing, the $\uparrow\downarrow$ and $\downarrow\uparrow$ parts of the self-energy and coupling matrices are zero. Thus, we can write the self-energy and gamma matrices as:

$$\Sigma_{L/R}(E) = \begin{pmatrix} \Sigma^{\uparrow}_{L/R} & 0 \\ 0 & \Sigma^{\downarrow}_{L/R} \end{pmatrix} \quad (19)$$

$$\Gamma_{L/R}(E) = \begin{pmatrix} \Gamma^{\uparrow}_{L/R} & 0 \\ 0 & \Gamma^{\downarrow}_{L/R} \end{pmatrix}. \quad (20)$$

Substituting those equations in the transmission function—Eq. (16), we have the spin resolved transmittance:

$$T^{\sigma_1\sigma_2}(E) = Tr\big[\Gamma^{\sigma_1}_L(E)(g^A_{cc}(E))^{\sigma_1\sigma_2}\Gamma^{\sigma_2}_R(E)(g^R_{cc}(E))^{\sigma_1\sigma_2}\big], \quad (21)$$

where $\sigma_1 = \sigma_2 = \uparrow,\downarrow$.

Results and Discussion

PRISTINE (3,0) GNR

We initially consider the charge transport through a pristine (3,0) GNR. As is well known, the zigzag nanoribbons present a spin-polarization at the edges, with a FM coupling along the ribbon direction. Between the edges the coupling can be either FM or AFM. In this work, we only consider the FM interedge coupling, which leads to a metallic behavior. We study two types of leads configurations: one where both leads have the same spin alignment [which will be called from now on FM configuration, see Fig. 2(a)] and another where the left and right leads have antiparallel alignments [which will be called from now on AFM configuration, see Fig. 2(b)].

In Figure 3(a) we show the spin-polarized bias-dependent IxV curve for the FM configuration. For a bias between −0.2V and +0.2V we verify that the current for both the majority and minority spins are degenerate and present a linear behavior. However, below and above this interval there is a splitting between the spin-up and spin-down currents. Because of this behavior zigzag GNRs with FM configuration could operate as spin-valves, as discussed in [6]. The reason for

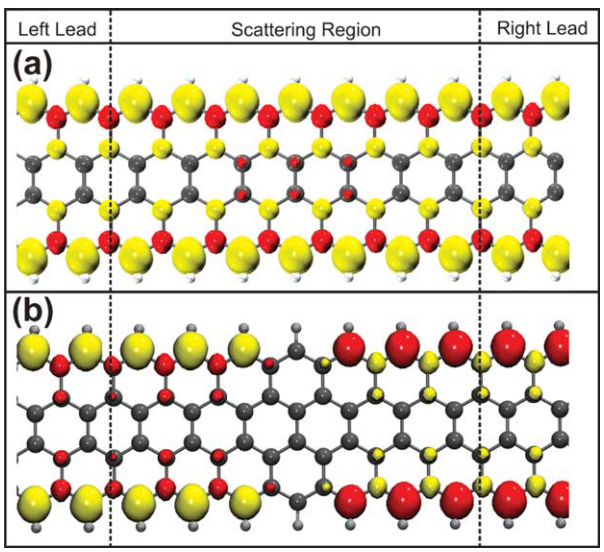

FIGURE 2. Configuration used for the transport calculations with the leads in (a) a parallel spin alignment (FM configuration) and (b) an antiparallel spin alignment (AFM configuration). [Color figure can be viewed in the online issue, which is available at wileyonlinelibrary.com.]

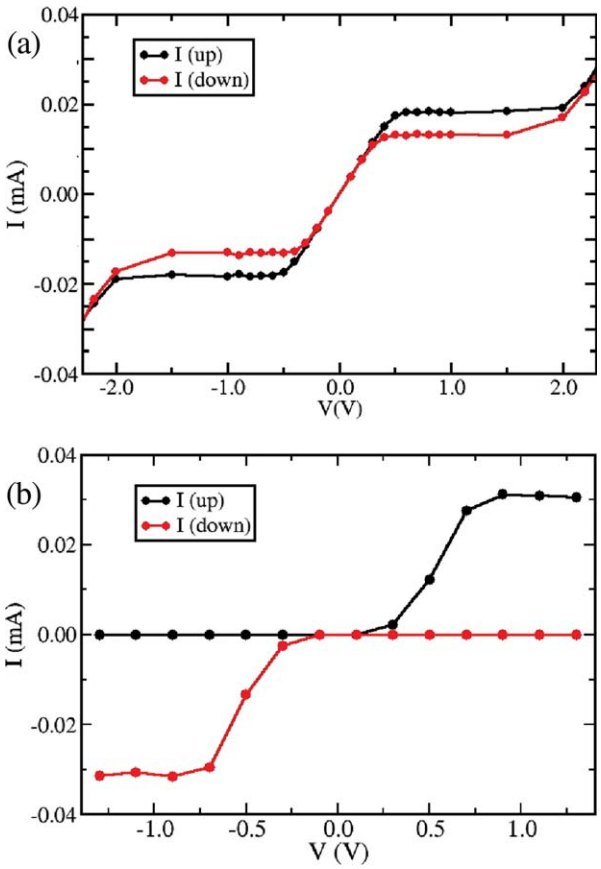

FIGURE 3. Spin polarized IxV curves for a pristine (3,0) graphene nanoribbon with the leads in the (a) FM configuration and (b) AFM configuration. The black (red) curve is the current for spin-up (spin-down). [Color figure can be viewed in the online issue, which is available at wileyonlinelibrary.com.]

this behavior is that for small bias the up and down spin transmittances are identical in the energy window where the left and right electrodes Fermi-Dirac distributions are distinct whereas for larger bias this is not so [see Eq. (15)].

For the AFM configuration we observe a spin-filter effect [Fig. 3(b)], with the current being, as expected, symmetric around zero bias if we consider the behavior of up and down spins. This behavior can be explained if we look at how the up and down transmittances vary with bias (see Fig. 4). For zero bias we verify that both spin states have an identical transmittance gap around the Fermi level. However, as a positive bias is applied, the transmittance gap decreases for the up spin whereas it increases for the down spin, leading to the spin-filter effect observed in Figure 3(b). Of course a similar behavior will occur for negative bias, but with the roles between up and down spins interchanged.

BORON AND NITROGEN DOPING GNR

Zigzag GNRs doped with Boron and Nitrogen have been widely discussed in the literature [14, 28–30]. The energetically most stable conformation has these atoms substituting a carbon atom right at the edge of the GNR, as shown in Figure 1. We calculated the spin polarized IxV curves for doped (3,0) GNRs with the leads always in the FM configuration.

The spin-polarized IxV curve for boron doping GNR is presented in Figure 5(a). We observe that the system has a difference between the spin currents indicating that it can function as a spin filter device. Moreover, there is an inversion between the up and down spin currents around a bias voltage of ± 1 V.

To understand this behavior in Figure 5 we plot the transmittances and the projected density of states on the carbon (edge and bulk-like) atoms for the three device regions: right lead, scattering region and left lead as well as on the boron atom. We present these results for 0.0V [Fig. 5(b)], +0.5V [Fig. 5(c)] and +1.5V [Fig. 5(d)]. From Figure 5(b) we can see that the boron states for down spins are more localized than the boron states for the up spins [14]. As a consequence, close to the Fermi level the majority spins are more scattered than the minority ones. Thus, the transmittance for down spins is higher than that for up spins. The spin polarization calculated as $P = \frac{T_\uparrow - T_\downarrow}{T_\uparrow + T_\downarrow}$, at the Fermi level, was -0.16.

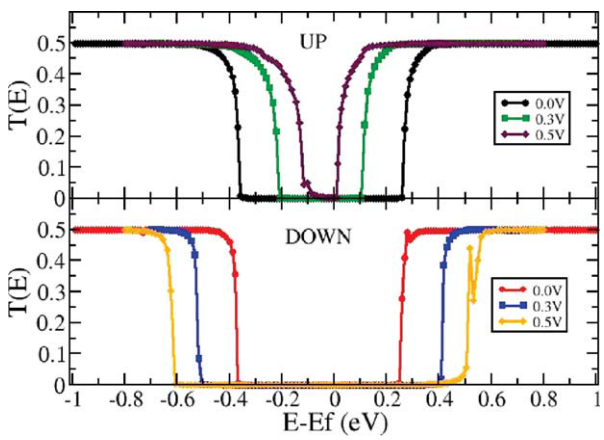

FIGURE 4. Transmittance, for spin-up and down, as a function of the bias voltage for the AFM configuration. [Color figure can be viewed in the online issue, which is available at wileyonlinelibrary.com.]

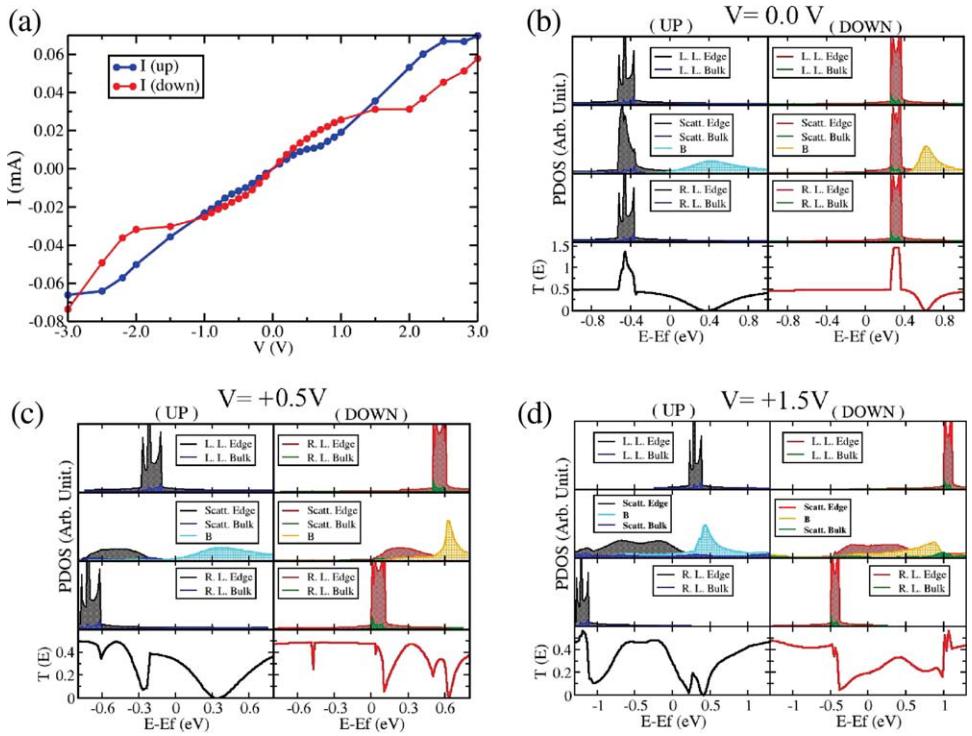

FIGURE 5. (a) Spin polarized IxV curve for boron doped graphene nanoribbon. The blue (red) curve is the current for spin up (down). Projected density of states and transmittance curves for different bias voltages: (b) 0.0 V; (c) +0.5 V; and (d) +1.5V. [Color figure can be viewed in the online issue, which is available at wileyonlinelibrary.com.]

As can be seen from Figure 5(c), this picture remains valid for bias voltages below approximately +1.0 V, with the boron down states still more localized than the boron up states, so the transmittance for the down channel is still greater than the up channels. Consequently, as can be seen in Figure 5(a), for a bias voltage of +0.5V, the current for down spin is greater than that for up spin. Increasing the bias voltage to +1.5V, we have an inversion of this picture, now the up spins are more localized then down states and as consequence the current for up spin is greater then for down spin. The same way of thinking can be used to explain the negative bias voltage.

For nitrogen doping the (3,0) monohydrogenated zigzag GNRs one electron is transferred to system, i.e., the localized nitrogen states for each spin component appear bellow the Fermi level. In Figures 6(a–d) we present the spin-dependent IxV curves, the projected density of states and the transmittance curves for different bias voltages. For zero bias transmittance [Fig. 6(b)] the spin polarization calculated, at the Fermi level, was 0.08, being T_{up} greater than T_{down}. As we are dealing with an impurity that introduces electrons, the spin up impurity states will show less dispersion than the spins down ones [28]. This characteristic can be verified in the PDOS for the nitrogen atom [Fig. 6(b)]. When a bias voltage of +0.5V is applied we verify that the overall transmittance for spin up is still greater than for spin down, and thus the current for spin up is also greater than for spin down. However, when a +1.0V bias voltage is applied the current is inverted; current for spin up is greater than current down. This is a combination of a variety of scattering and interference effects related both to the nitrogen as well as the localized edge states.

Summary

In summary, we have performed *ab initio* electronic structure and transport calculations for pristine (3,0) zigzag GNRs with the leads having either a parallel (FM) or antiparallel (AFM) magnetization, as well as for GNRs doped with boron or nitrogen. For the pristine system with leads in the FM configuration, due to the constant values of the transmittance around the Fermi level, the

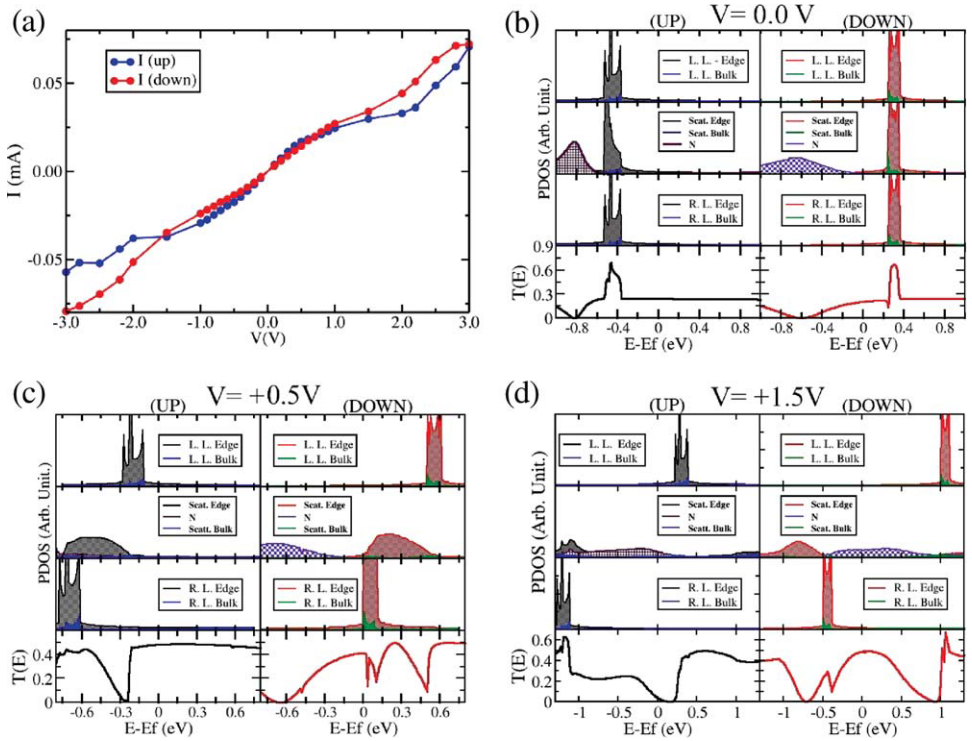

FIGURE 6. (a) Spin polarized IxV curve for nitrogen doped graphene nanoribbon. The blue (red) curve is the current for spin up (down). Projected density of states and transmittance curves for different bias voltages: (b) 0.0 V; (c) +0.5 V; and (d) +1.5V. [Color figure can be viewed in the online issue, which is available at wileyonlinelibrary.com.]

current for low bias presents a linear behavior. Moreover, both the up and down spin currents are the same. However, for biases between +(-) 0.5V and +(-) 2.0V, the currents are almost constant and the up and down currents are nondegenerated. Analyzing the pristine AFM configuration we verify that it presents a spin filter effect, with the current being transported by only one spin carrier, either for positive or negative bias. Doping the system with boron and nitrogen leads to a nondegenerated current along all the bias voltages investigated (leads always in the FM configuration). For the boron, with low positive bias, the down current is bigger than the up one, whereas for nitrogen we observe the opposite behavior. This is due to the fact that boron adds a hole to the system whereas nitrogen adds an electron. For both boron and nitrogen doping we observe an inversion of the spin polarization above and below some threshold value of the bias voltage.

ACKNOWLEDGMENT

The authors congratulate Prof. Sylvio Canuto for his 60th birthday.

References

1. Novoselov, K. S.; Geim, A. K.; Morozov, S. V.; Jiang, D.; Katsnelson, M. I.; Grigoreva, V.; Dubonos, S. V.; Firsov, A. A. Nature 2005, 438, 197.
2. Zhang, Y.; Tan, Y.-W.; Stormer, H. L.; Kim, P. Nature 2005, 438, 201.
3. Stankovich, S.; Dikin, D. A.; Dommett, G. H. B.; Kohlhaas, K. M.; Zimney, E. J.; Stach, E. A.; Piner, R. D.; Nguyen, S. T.; Ruoff, R. S. Nature 2006, 442, 282.
4. Fiori, G.; Iannaccone, G. IEEE Electron Device Lett 2007, 28, 760.
5. Liang, G.; Neophytou, N.; Lundstron, M. S.; Nikonov, D. E. J Appl Phys 2007, 102, 054307.
6. Kim, W. Y.; Kim, K. S. Nat Nanotechnol 2008, 3, 408.
7. Han, M. Y.; Özyilmaz, B.; Zhang, Y.; Kim, P. Phys Rev Lett 2007, 98, 206805.
8. Son, Y. W.; Cohen, M. L.; Louie, S. G. Nature 2006, 444, 347.
9. Pisani, L.; Chan, J. A.; Montanari, B.; Harrison, N. M. Phys Rev B 2007, 75, 064418.
10. Tapaszto, L.; Dobrik, G.; Lambin, P.; Biro, L. P. Nat Nanotechnol 2008, 3, 397.
11. (a) Pantelides, S. T. Rev Mod Phys 1978, 50, 798; (b) Mieghem, P. V. Rev Mod Phys 1992, 64, 755.

12. (a) Ho, J. C.; Yerushalmi, R.; Jacobson, Z. A.; Fan, Z.; Alley, R. L.; Javey, A. Nat Mater 2008, 7, 62; (b) Jung, N.; Kim, N.; Jockusch, S.; Turro, N. J.; Kim, P.; Brus, L. Nano Lett 2009, 12, 4133; (c) Norris, D. J.; Efros, A. L.; Erwin, S. C. Science 2008, 319, 17176.
13. Cunha, C.; Canuto, S.; Fazzio, A. Phys Rev B 1993, 48, 17806.
14. Martins, T. B.; Miwa, R. H.; da Silva, A. J. R.; Fazzio, A. Phys Rev Lett 2007, 98, 196803.
15. Ezawa, M. Phys Rev B 2006, 73, 045432.
16. Hohenberg, P.; Kohn, W. Phys Rev 1964, 136, B864.
17. Kohn, W.; Sham, L. J. Phys Rev 1965, 140, A1133.
18. Perdew, J. P.; Burke, K.; Ernzerhof, M. Phys Rev Lett 1996, 77, 3865.
19. Troullier, N.; Martins, J. L. Phys Rev B 1991, 43, 1993.
20. Soler, J. M.; Artacho, E.; Gale, J. D.; García, A.; Junquera, J.; Ordejón, P. and Sánchez-Portal, D. J. Phys Condens Matter 2002, 14, 2745.
21. Monkhorst, H. J.; Pack, J. D. Phys Rev B 1976, 13, 5188.
22. (a) Taylor, J.; Guo, H.; Wang, J. Phys Rev B 2001, 63 245407; (b) Xue, Y.; Datta, S.; Ratner, M. A. Chem Phys 2002, 281, 151.
23. Novaes, F. D.; da Silva, A. J. R.; Fazzio, A. Braz J Phys 2006, 36, 799.
24. Datta, S. Quantum Transport: Atom to Transistor, Cambridge University Press, Cambridge, 2005.
25. Brandbyge, M.; Stokbro, K.; Taylor, J.; Mozos, J. L.; Ordejón, P. Material Research Society Symposium Proceedings 2000, 636, D9.25.
26. di Ventra, M. Electrical Transport in Nanoscale Systems; Cambridge University Press: Cambridge, 2008.
27. Meir, Y.; Wingreen, N. S. Phys Rev Lett 1992, 68, 2512.
28. Martins, T. B.; da Silva, A. J. R.; Miwa, R. H.; Fazzio, A. Nano Lett 2008, 8, 2293.
29. Zheng, X. H.; Rungger, I.; Zeng, Z.; Sanvito, S. Phys Rev B 2009, 80, 235426.
30. Dutta, S.; Manna, A. K.; Pati, S. K. Phys Rev Lett 2009, 102: 096601.